Numerical Study of Facility Effects on Gridded Ion Thrusters through a Multi-GPU PIC-DSMC Solver

IEPC-2024-323

Presented at the 38th International Electric Propulsion Conference, Toulouse, France
June 23-28, 2024

Keita Nishii*
Tokyo Metropolitan University, Hino, Tokyo, 1910065, Japan

Deborah A. Levin†
University of Illinois Urbana-Champaign, Urbana, Illinois, 61801, USA

This study investigates the facility effects on gridded ion thrusters tested in ground vacuum chambers using a Multi-GPU PIC-DSMC solver, CHAOS. The research summarizes our recent work on contamination by backsputtered particles and the coupling between the electron source and chamber walls. These results indicate that different sputter models significantly impact backsputtering rates and that ground-based conditions alter electron temperatures and potentials compared to space conditions. In addition. dimensional scaling is applied to reduce computational costs for a vacuum chamber simulation, revealing that potential and electron energy are underestimated. These findings provide fundamental results useful for future numerical studies on facility effects.

I. Introduction

Gridded ion thrusters are tested in ground vacuum chambers to verify their performance when operated in space. However, the presence of high background pressure and conductive walls in the vacuum chamber leads to facility effects that increase uncertainty in the performance of the thruster in space. Typical operating chamber pressures are approximately three orders or more of magnitude higher than the ambient gas pressures of 10^{-9} Torr on orbit (at 1000 km). At such high background pressure, the lifetime of ion grid optics is impacted by erosion driven by charge exchange (CEX) ions. Another limitation is the surrounding wall of the vacuum chamber. The high energy ion bombardment on the wall sputters wall material, and its deposition masks erosion caused by CEX backflow ions. Thus, the understanding of backsputtering in the vacuum chamber is essential, and there are several studies modeling sputtered particles.[1,2]

In addition, ion beam neutralization depends on the neutralizer to ion beam plasma bridge, which can be affected by nearby wall surfaces and CEX collisions. For such reasons, it is important to understand the interaction between the thruster plasma plume and the ground facility. Several numerical simulations have been performed to understand ion beam neutralion.[3–7] Plasma plumes from thrusters are mostly measured in laboratories, with limited direct measurements in space.[8,9] Therefore, comparing ground-based and space-based conditions through numerical simulations is a highly effective approach to understanding facility effects. This method allows researchers to bridge the gap between laboratory measurements and on-orbit performance, providing insights into the interactions between the thruster plasma plume and the testing environment.

Investigating facility effects requires accounting for neutral particles, ions, and electrons, and the large computational domain necessitates significant parallelization for speed. We have developed an in-house code, Cuda-based Hybrid Approach for Octree Simulations (CHAOS), which features adaptive mesh refinement with octree mesh and is accelerated using MPI-CUDA parallelization strategies. This code has been employed not only for the current study but also for simulating multiphase flows[10] and investigating electron solitary

*Assistant Professor, Department of Aeronautics and Astronautics, knishii@tmu.ac.jp
†Professor, Department of Aerospace Engineering, deblevin@illinois.edu

Copyright 2024 by the Electric Rocket Propulsion Society. All rights reserved.

wave dynamics.[11] The advanced capabilities of CHAOS make it well-suited for addressing the complex interactions in ion thruster plume simulations.

In the next chapter, we report our numerical work on contamination due to particles sputtered from a vacuum chamber wall[12] (i.e., backsputtering facility effects) and coupling between the electron source and the wall[13] (i.e., electrical facility effects). For backsputtering, we examine the importance of a sputtering model for carbon particles when fast xenon ions hit the wall (Section A). For electrical facility effects, we examine how the amount of current changes with and without the wall surface and with and without the background gas (Section B).

However, these studies have been performed with plasma densities 10–100 times smaller than those of actual ion thrusters. This is because it is not possible to perform a full-kinetic simulation of the entire vacuum chamber on a realistic scale, due to the limitations of current computational resources. To overcome this limitation, dimensional scaling has been used in a few cases to calculate ion thrusters.[4,14,15] In this study, we also discuss what results are obtained when dimensional scaling is applied to an ion thruster plume in a vacuum chamber (Section IV). These results may be useful for future numerical studies on facility effects.

II. Highlights of our Facility Effect Study

A. Backsputtering Simulation

The work[12] simulated an ion thruster plume using both fully kinetic and quasi-neutral Boltzmann models. Here, the kinetic model means that electrons are treated as particles, and the electric potential is calculated based on Poisson's equation. The Boltzmann model treats electrons as fluid, and the electric potential is calculated based on the Boltzmann relation equation. The work investigated the impact on flux, energy, and angle of incident ions on chamber walls (see Fig. 10 in Ref.[12]). For momentum exchange (MEX) ions (top plots), there was almost no difference between the fully kinetic and Boltzmann cases in terms of flux, incident energy, and angle. This was because MEX ions had high initial energies, making electric potential differences less impactful. As distance increased, the flux and energy of MEX ions rose due to their larger z velocities. In contrast, CEX ions (bottom plots) showed significant differences between the fully kinetic and Boltzmann cases. CEX ions, which initially had small velocities, gained energy from the electric potential and moved along the electric field. The fully kinetic simulation predicted higher incident energy and a wider incident angle distribution compared to the Boltzmann case, attributed to the potential barrier in the Boltzmann case, which reduced CEX ion energy, especially near the thruster exit. Additionally, in the Boltzmann case, CEX ions moved behind the thruster where ion density was lower, affecting their incident angles.

The study[12] also explored how different sputter models affect the spatial distribution and deposition rate of carbon backsputtered onto the ion thruster face. Sputtering, caused by high-energy beam ions impacting downstream walls, was evaluated using the cosine distribution and Yim's model.[16,17] The work showed that high-energy ions, such as MEX ions, had sufficient energy to cause sputtering, with no significant difference between the fully kinetic and Boltzmann cases for these ions (see Fig. 17 in Ref.[12]). The influence of electric field modeling on backsputtering was negligible due to the lower flux and energy of CEX ions compared to beam ions.

In conclusion, the choice of the sputter model significantly impacted predicted carbon backsputtering rates. Yim's model,[16,17] based on experimental data, appears to offer a more accurate representation, emphasizing the need for realistic angular dependence in sputtering models to better predict and mitigate backsputtering effects in ion thrusters. How sputtering models are underdeveloped and will be considered in the future.[18]

B. Electrical Facility Effect Simulation

Another work[13] investigated the electrical facility effect using a fully kinetic model. The comparison between space and ground-based conditions showed higher electron temperatures and potential in ground-based simulations due to electron absorption by chamber walls, contrasting with space simulations where electrons were reflected back. Table 1 (Table 6 in Ref.[13]) highlighted significant differences in electron currents: the grounded chamber walls increased electron currents to the plasma screen and decreased currents escaping the chamber. These findings suggested that ground tests may underestimate the electron currents returning to the thruster, impacting the accuracy of ground-based thruster performance predictions.

The study also examined the impact of background pressure in a vacuum chamber on ion thruster

Copyright 2024 by the Electric Rocket Propulsion Society. All rights reserved.

Table 1. Ion and electron current from thruster plume to different locations. (from Nishii and Levin[13])

Case	Ion Current, I_i/I_{i0}^b				Electron Current, I_e/I_{e0}^b			
	I_{ne}	I_{th}	I_{ps}	$I_{vc}(=I_{vc,end}+I_{vc,side})$	I_{ne}	I_{th}	I_{ps}	$I_{vc}(=I_{vc,end}+I_{vc,side})$
Space	0.00	0.00	0.01	0.99	0.39	0.06	0.26	0.29
Chamber (w/o BP[a])	0.00	0.00	0.01	0.99 (= 0.99 + 0.00)	0.18	0.01	0.02	0.78 (= 0.59 + 0.19)
Chamber (w/ BP[a])	0.00	0.01	0.02	0.96 (= 0.72 + 0.24)	0.14	0.01	0.05	0.79 (= 0.57 + 0.22)

[a] BP indicates the background pressure.

[b] See Fig. 3 in Ref.[13] for definitions of the current to each part.

plumes. The presence of neutral particles at typical ground test pressures led to the formation of slow charge-exchange ions, which increased ion density and reduced the electric potential in the plume, resulting in improved plume neutralization. Additionally, these ions created ion sheaths near the chamber walls, altering ion current paths. The study found that background pressure effects must be considered to simulate and predict ion thruster performance in ground-based tests accurately.

In conclusion, ground-based vacuum chamber tests significantly affect ion thruster plume characteristics, increasing electron temperature and altering current paths due to grounded walls and background pressure. Accurate predictions of on-orbit performance require accounting for these facility effects in simulation and testing methodologies.

III. Simulation Code: CHAOS

A. DSMC and PIC Modules

The CHAOS framework utilizes direct simulation Monte Carlo (DSMC), particle-in-cell (PIC), and gas surface interaction (GSI) modules to simulate ion thruster plasma plumes accurately.[6,7,12,13,19,20] Figure 1 shows the flowchart between three major modules in the code. The DSMC module is primarily responsible for modeling three types of collisions: momentum exchange (MEX) collisions between xenon neutral particles and ions, and CEX collisions between xenon ions and neutral particles. In this module, particle interactions are performed within the leaf nodes of an octree grid, where particles are mapped to these nodes, and collisions are computed using a no-time counter (NTC) collision scheme. This method is particularly effective in accounting for the different timescales and weighting factors of ions and neutrals, ensuring accurate modeling of collision dynamics within the plasma plume.

The main objective of the PIC module is to calculate the self-consistent electric field based on the spatial distribution of charged particles. This is achieved by solving Poisson's equation on an unstructured octree grid using the preconditioned conjugate gradient (PCG) method. The electric potential is iteratively computed until convergence is achieved, after which the electric field is derived. The octree grid is refined adaptively to ensure that the cell size is smaller than the local Debye length, maintaining the accuracy of the electric field calculations. The PIC module operates in conjunction with the DSMC module, providing the necessary electric field data to update the velocities and accelerations of charged particles.

In our recent work,[12,13] we have extended CHAOS to model ground facility environments, focusing on two critical plasma-surface interactions: charge absorption and sputtering as the GSI module. When ions hit the wall, they lose their positive charge and become neutralized. This process significantly affects the background pressure distribution. Additionally, modeling sputtered particles from the vacuum chamber walls is a key objective. When high-energy ions impact the walls, they cause material sputtering, which must be accurately simulated to understand contamination and erosion effects. By incorporating these interactions, CHAOS can more precisely replicate the conditions and challenges faced by ion thrusters in ground-based testing environments.

B. PIC-DSMC Coupling

The CHAOS framework employs a sophisticated coupling methodology to integrate the PIC and DSMC modules effectively.[7,12,13,20] This coupling is necessary to handle the disparate time and length scales associated with collisions and electric field evolution in ion thruster plumes. Key strategies employed in this

Copyright 2024 by the Electric Rocket Propulsion Society. All rights reserved.

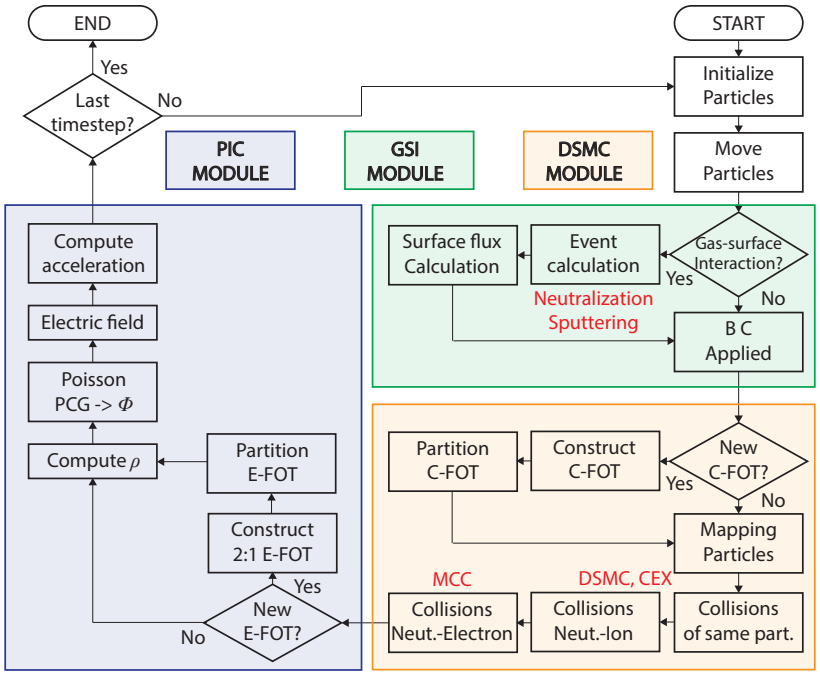

Figure 1. Schematic diagram of the relationship between major modules in CHAOS

coupling include as follows.

1. *Separated Octree Grids*

CHAOS constructs two distinct octree grids for the DSMC and PIC simulations, referred to as the collision-forest of trees (C-FOT) and electric-field forest of trees (E-FOT), respectively. The C-FOT is designed to resolve local mean free paths for collision calculations, while the E-FOT resolves local Debye lengths for electric field calculations. These grids are dynamically refined and linearized to optimize computational efficiency and accuracy.

2. *Species Timestep and Weighting Factors*

To handle the different densities and velocities of ions, electrons, and neutrals, CHAOS employs species-specific timesteps and weighting factors. Neutrals are moved only during DSMC executions, while ions and electrons are updated every PIC iteration. Weighting factors increase the number of computational particles for charged species, ensuring sufficient particle counts for accurate collision statistics and electric field computations.

3. *Time-Slicing for Disparate Timescales*

Given the significant difference in timescales between collisions and electric field evolution, the DSMC module is executed less frequently than the PIC module. Typically, the DSMC module is called after several hundred PIC iterations, allowing the PIC module to update the electric field more frequently and accurately. This approach ensures that the DSMC collisions are performed over appropriate timescales without unnecessary computational expense.

4. *Decoupled sampling*

For steady-state simulations, the electric field is established relatively fast. At that point, the computationally intensive PIC module, which calculates the electric field based on the spatial distribution of charged particles, is no longer invoked. Instead, the steady-state electric field is sampled and used for further calculations. After decoupling, the DSMC module continues to simulate heavy particle collisions with the velocities and

Copyright 2024 by the Electric Rocket Propulsion Society. All rights reserved.

positions of the charged ions updated using the steady-state electric field obtained earlier. This step allows the simulation to focus on collision dynamics, such as MEX and CEX collisions, without the need to recalculate the electric field at every iteration.

IV. Dimensional Scaling

A. Simulation conditions

Dimensional scaling aims to reduce computational costs by using a scaling factor, f, to decrease the actual dimensions of the computational domains. In this case, for three-dimensional calculation, since the particle flux is kept constant, the total number of computational particles decreases by $1/f^3$. Additionally, the number of time steps required to reach a steady state becomes $1/f$, which results in an approximately $1/f^4$ reduction in computational cost. Note that scaling will change plasma dynamics, especially near the walls, since the Debye length does not change by this dimensional scaling. When considering collisions of neutral particles or the effects of external electric and magnetic fields, the scaling scheme in Ref.[14] can be used. In our study, these effects were ignored, and only ions and electrons were simulated.

Generally, the influence of the size and plasma density at the exit of the ion engine is characterized by the ratio of the thruster exit radius to the Debye length based on the exit plasma density (R_0/λ_0).[13,15] The maximum R_0/λ_0 of Ref[12] and Ref.[13] were 285 and 19, respectively. In our work, to address the actual scale, the ion density of 2.62×10^{15} m^{-3} was determined based on the ion flux and velocity in Ref.,[21] as shown in Table 2. The electron temperature was set to 2 eV, and the electron density was determined so that the ion-to-electron current ratio was the same as that of Ref.[12] and Ref.[13] The Debye length at the thruster exit was 2.1×10^{-4} m in this condition.

Table 2. Species setting on the thruster exit for scaling study based on Ref.[21]

Species at thruster exit	Xe^+	e^-
Current, mA	80.9	250
Flux, $m^2 \cdot s$	1.0×10^{20}	3.1×10^{20}
Number density, m^{-3}	2.62×10^{15}	9.84×10^{14}
Bulk velocity, m/s	38,338	0
Temperature, K	0 (12° Gaussian dist.)	23,210 (2 eV)

To investigate the effect of dimensional scaling, we set the test geometry shown in Fig. 2. The ion thruster was placed on the left-hand side at a distance from the vacuum chamber downstream wall of 10 cm, and the electrical potential of the vacuum chamber and thruster were set at 0 V. Similar to Ref.,[12] this study only simulates a quarter domain due to symmetry to further save computational effort. We tested four scaling factors: 1 (baseline), 2, 4, and, 8. The dimensions and simulation parameters for each scaling factor are displayed in Table 3. In the baseline case, since the exit radius was 4 cm, $R_0/\lambda_0 = 1904$. Due to the large number of cells required, the number of computed particles was 520 M/species, and the required resources were 32 Nvidia A100 GPUs. As a result of scaling, the number of total computational particles decreased by a factor of $1/f^3$. At $f = 8$, $R_0/\lambda_0 = 238$, where the Debye length at the thruster exit was still small enough compared to the thruster dimension. For computational parameters, a timestep of 4.0×10^{-11} and F_{num} of 6.25×10^2 were selected. Once the number of computational particles reached almost steady (at 100,000 timesteps for the baseline case), we started the steady result sampling.

B. Results and Discussion

Figure 3 shows the two-dimensional electric potential result for all scaling factors. The potential decreased as f increased. In the baseline (f=1) case, the maximum potential was approximately 9.5 V. In the f=8 case, the maximum potential was approximately 6 V. Since the mesh size was adjusted to a size slightly smaller than the Debye length by adaptive mesh refinement, the computational mesh was coarser for larger scaling factors.

The electric potential, ion number density, and electron number density on the thruster center axis ($y/D = 0.0$) and cross-stream direction ($z/D = 1.875$) are shown in Fig. 4 to provide a qualitative comparison. The

Copyright 2024 by the Electric Rocket Propulsion Society. All rights reserved.

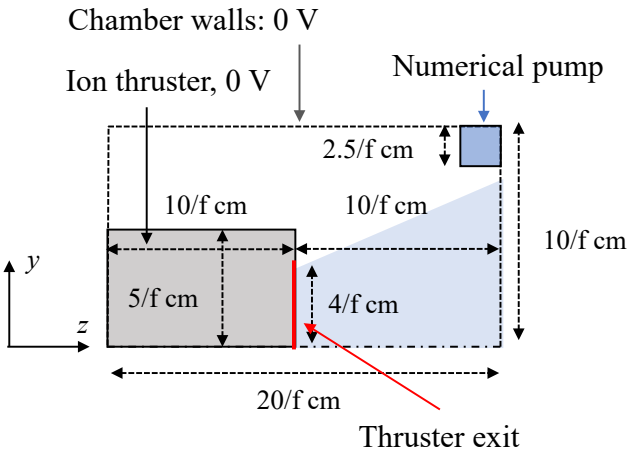

Figure 2. Geometry for a scaling study.

Table 3. Dimensions and simulation parameters for each scaling factor.

Scaling factor, f	1 (baseline)	2	4	8
Domain size, cm	(10, 10, 20)	(5, 5, 10)	(2.5, 2.5, 5)	(1.25, 1.25, 2.5)
Thruster size, cm	(5, 5, 10)	(2.5, 2.5, 5)	(1.25, 1.25, 2.5)	(0.725, 0.725, 1.25)
Exit radius, cm	4	2	1	0.5
Pump size, cm	2.5	1.25	0.725	0.3125
R_0/λ_0	1905	952	476	238
Total particles / species	520 M	65 M	8 M	1 M

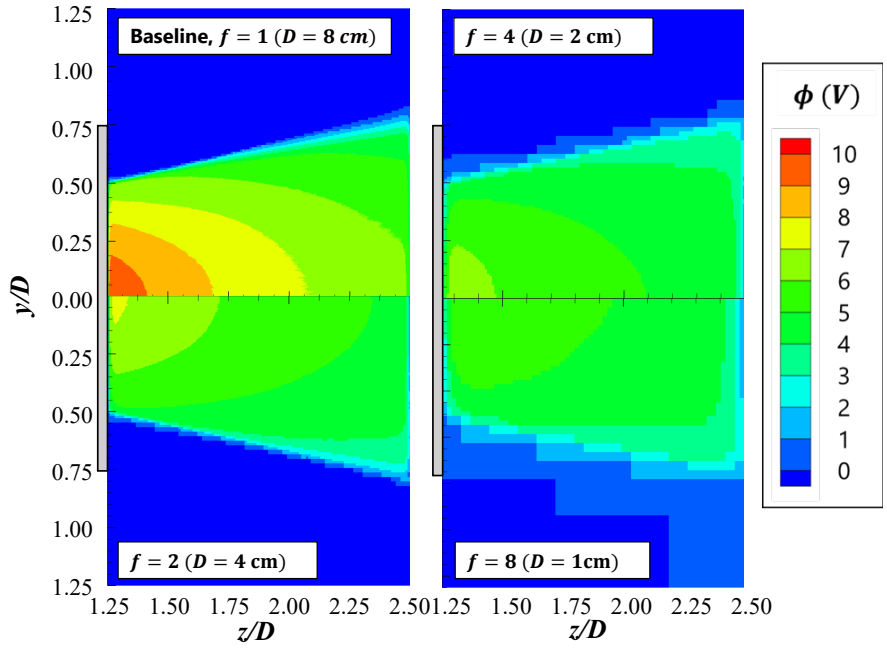

Figure 3. Electric potential contours at scaling factors of 1, 2, 4, and 8.

left plot shows the potential curves. Due to the boundary conditions, the potential along the wall at $z/D = 1.25$ and $z/D = 2.50$ has a fixed potential of 0 V and reaches its maximum value downstream of the thruster. As can be seen in Fig. 3, the potential becomes lower as the scaling factor is increased. On the

Copyright 2024 by the Electric Rocket Propulsion Society. All rights reserved.

other hand, for the ion and electron densities, the difference due to the scaling factor was small.

In addition, Fig. 5 shows the electric potential, ion number density, and electron number density in the cross-stream direction ($z/D = 1.875$). In the left potential plot, a negative potential is seen in the region outside the ion beam ($0.7 < y/D < 1.1$) in the baseline case. This is due to the formation of an "electron pool" because ions have a lower temperature, whereas electrons have a higher temperature and can move outside the region where the ion beam is present. Interestingly, this negative potential disappears as f is increased. There are small differences between the ion and electron densities, similar to the results for the thruster axial direction. For electron density, as f is increased, the gradient at the edge of the ion beam ($y/D \sim 0.6$) becomes smoother, and abrupt changes in potential are not captured.

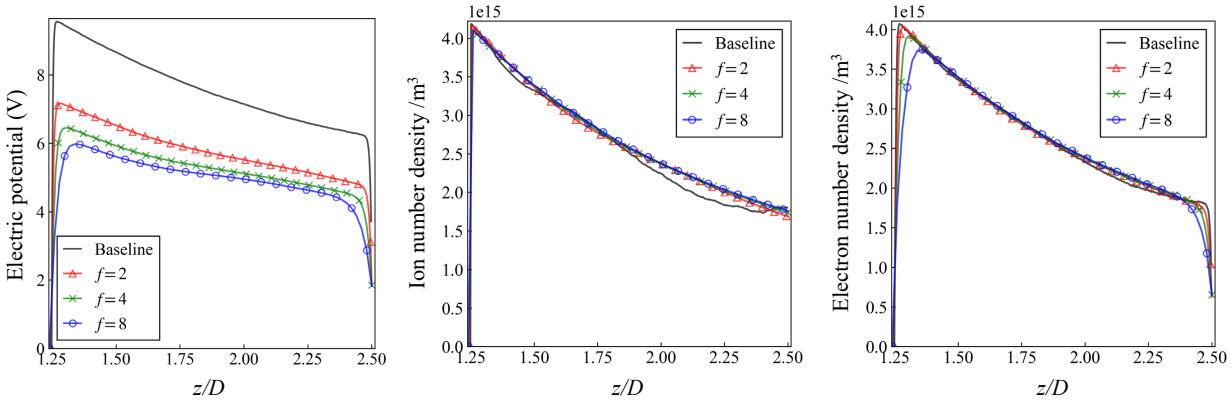

Figure 4. Thruster axis results of potential, ion density, and electron density.

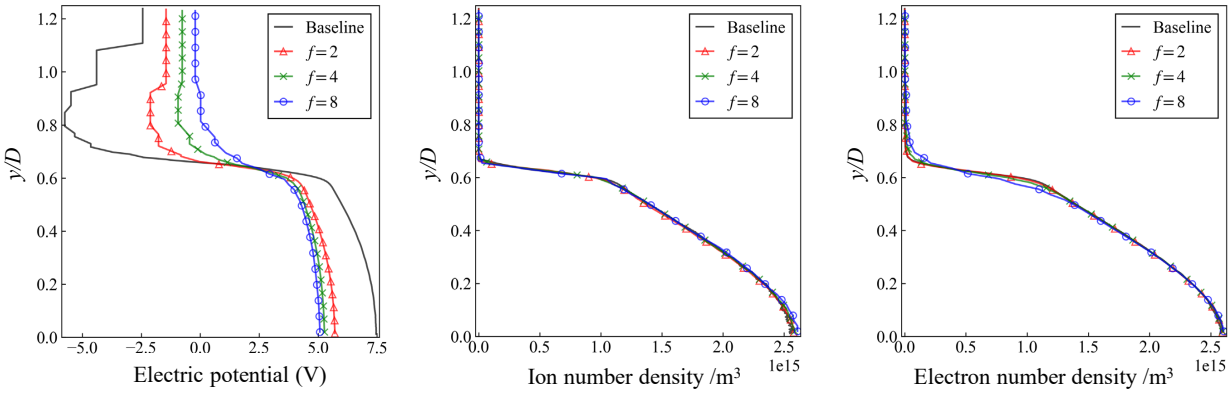

Figure 5. Y-direction results of potential, ion density, and electron density at $z/D = 1.875$.

Finally, the electron energy distributions at the center of the plume $(y/D, z/D) = (0.0, 1.88)$, and near the downstream of the wall $(y/D, z/D) = (0.0, 2.45)$ were obtained, as shown in Fig. 6. This figure shows that the mean energy and the width of the electron distribution (i.e., temperature) are greatly reduced by the scaling process and probably cause the reduction of the potentials in Fig. 3. The scaling-induced changes observed here are attributed to the smaller length plasma scale without changing the Debye length, which results in a smaller shielding effect. However, it should be noted that for simulations where the chamber and thruster walls play a small role (e.g., plume core regions), Figs. 4 and 5 show that such a scaling appears given a good estimate of species profiles.

V. Conclusion

This research provides critical insights into the facility effects on gridded ion thrusters tested in ground vacuum chambers. Using the CHAOS code, which integrates DSMC and PIC modules, we explored the

Copyright 2024 by the Electric Rocket Propulsion Society. All rights reserved.

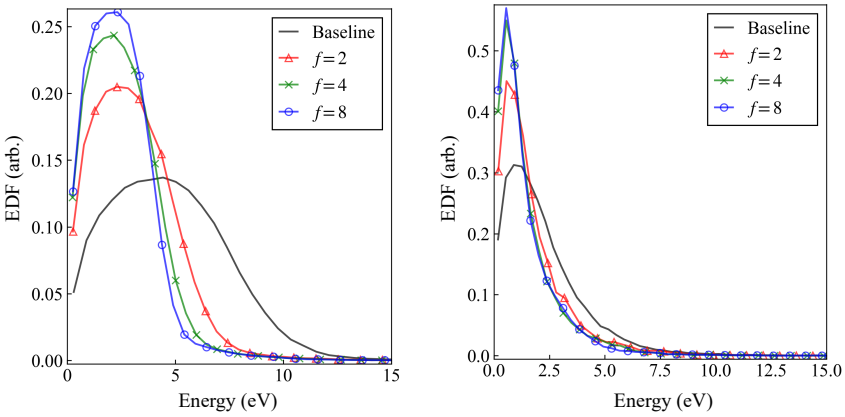

Figure 6. Electron energy distribution function sampled by a numerical probe, (a) at $y/D = 0.0$ and $z/D = 1.88$, (b) at $y/D = 0.0$ and $z/D = 2.45$,

impacts of backsputtering and electrical facility effects. Our findings show that different sputter models, particularly, provide more accurate predictions of carbon backsputtering rates compared to the cosine distribution. Furthermore, ground-based simulations revealed higher electron temperatures and potentials due to electron absorption by chamber walls, contrasting with space simulations where electrons are reflected. The presence of neutral particles at ground test pressures forms slow CEX ions, increasing ion density and reducing electric potential, thereby improving plume neutralization.

The use of dimensional scaling to reduce computational costs was also examined, showing that potential and electron energy are underestimated when scaling is applied. These results underscore the importance of considering facility effects in ground-based tests to ensure accurate predictions of ion thruster performance in space. For ion beams that already have large bulk velocities, these differences have little effect. However, since CEX ions have not been calculated in this study, the effect on CEX ions should be considered in the future.

Acknowledgments

This work was partially supported by NASA through the Joint Advanced Propulsion Institute, a NASA Space Technology Research Institute, grant number 80NSSC21K1118. This work used Delta at the National Center for Supercomputing Applications through allocation TG-PHY220010 from the Advanced Cyberinfrastructure Coordination Ecosystem: Services & Support (ACCESS) program, which is supported by National Science Foundation grants #2138259, #2138286, #2138307, #2137603, and #2138296.

References

[1]Zheng, H., Cai, G., Liu, L., Shang, S., and He, B., "Three-dimensional particle simulation of back-sputtered carbon in electric propulsion test facility," *Acta astronautica*, Vol. 132, March 2017, pp. 161–169.

[2]Araki, S. J. and Martin, R. S., "Sputtered atom transport calculation via Radiosity View Factor Model and particle data compression," *Vacuum*, Vol. 210, April 2023, pp. 111867.

[3]Usui, H., Hashimoto, A., and Miyake, Y., "Electron behavior in ion beam neutralization in electric propulsion: full particle-in-cell simulation," *Journal of physics. Conference series*, Vol. 454, No. 1, Aug. 2013, pp. 012017.

[4]Brieda, L. and Wang, J., "Modelling ion thruster beam neutralization," *AIAA Paper 2005-4045*, July 2005.

[5]Brieda, L., "Model for Steady-State Fully Kinetic Ion Beam Neutralization Studies," *IEEE transactions on plasma science*, Vol. 46, No. 3, March 2018, pp. 556–562.

[6]Jambunathan, R. and Levin, D. A., "CHAOS: An octree-based PIC-DSMC code for modeling of electron kinetic properties in a plasma plume using MPI-CUDA parallelization," *Journal of computational physics*, Vol. 373, Nov. 2018, pp. 571–604.

[7]Jambunathan, R. and Levin, D. A., "A Self-Consistent Open Boundary Condition for Fully Kinetic Plasma Thruster Plume Simulations," *IEEE transactions on plasma science*, Vol. 48, No. 3, March 2020, pp. 610–630.

[8]Kerslake, W. R. and Ignaczak, L. R., "SERTII1979-1981 Tests: Plasma Thrust and Neutralizer Measurements," *Journal of Spacecraft and Rockets*, Vol. 19, No. 3, May 1982, pp. 236–240.

Copyright 2024 by the Electric Rocket Propulsion Society. All rights reserved.

[9]Kerslake, W. R. and Ignaczak, L. R., "Development and flight history of the SERT II spacecraft," *Journal of Spacecraft and Rockets*, Vol. 30, No. 3, May 1993, pp. 258–290.

[10]Marayikkottu, A. V. and Levin, D. A., "Kinetic modeling of fluid-induced interactions in compressible, rarefied gas flows for aerodynamically interacting particles," *International Journal of Multiphase Flow*, Vol. 171, Jan. 2024, pp. 104684.

[11]Nuwal, N., Levin, D. A., and Kaganovich, I. D., "Kinetic modeling of solitary wave dynamics in a neutralizing ion beam," *Physics of plasmas*, Vol. 30, No. 1, Jan. 2023, pp. 012110.

[12]Nishii, K. and Levin, D. A., "Three-Dimensional Kinetic Simulations of Carbon Backsputtering in Vacuum Chambers from Ion Thruster Plumes," *Journal of Propulsion and Power*, Vol. 40, No. 1, Jan. 2024, pp. 123–137.

[13]Nishii, K. and Levin, D. A., "Kinetic simulation of ion thruster plume neutralization in a vacuum chamber," *Plasma Sources Science and Technology*, Vol. 32, No. 11, Nov. 2023, pp. 115009.

[14]Yuan, T., Ren, J., Zhou, J., Zhang, Z., Wang, Y., and Tang, H., "The effects of numerical acceleration techniques on PIC-MCC simulations of ion thrusters," *AIP advances*, Vol. 10, No. 4, April 2020, pp. 045115.

[15]Hu, Y., Wang, J., and Sun, Q., "Geometrically self-similar ion acceleration in collisionless plasma beam expansion," *Plasma Sources Science and Technology*, Vol. 29, No. 12, Dec. 2020, pp. 125004.

[16]Yim, J. T., "A Survey of Xenon Ion Sputter Yield Data and Fits Relevant To Electric Propulsion Spacecraft Integration," *Proceedings of the 35th International Electric Propulsion Conference*, IEPC-2017-060, October 2017.

[17]Yim, J. T., "Differential Yields and Uncertainty Assessments for Electric Propulsion Plume Impingement Sputter Redeposition Contamination," *Proceedings of the 37th International Electric Propulsion Conference*, IEPC-2022-580, June 2022.

[18]Lim, G., Nishii, K., Tran, H., Chew, H. B., and Levin, D. A., "Kinetic Simulation of Carbon Sputtering by a Gridded Ion Thruster with a Molecular Dynamics Based Model," *Proceedings of the 38th International Electric Propulsion Conference*, IEPC-2024-186, June 2024.

[19]Jambunathan, R. and Levin, D. A., "Kinetic, 3-D, PIC-DSMC Simulations of Ion Thruster Plumes and the Backflow Region," *IEEE transactions on plasma science*, Vol. 48, No. 6, June 2020, pp. 2017–2034.

[20]Nuwal, N., Jambunathan, R., and Levin, D. A., "Kinetic Modeling of Spacecraft Surfaces in a Plume Backflow Region," *IEEE transactions on plasma science*, Vol. 48, No. 12, Dec. 2020, pp. 4305–4325.

[21]Patterson, M., "Low-power ion thruster development status," *AIAA Paper 1998-3347*, July 1998.

Copyright 2024 by the Electric Rocket Propulsion Society. All rights reserved.